Department of Electrical and Computer Systems Engineering

Technical Report MECSE-12-2005

Photonic Signal Processing –Part II.2: Tunable Photonic Filters using Cascaded All-Pole Micro-rings and All-Zero Interferomers

Le Nguyen Binh

MONASH UNIVERSITY

Photonic Signal Processing – Part II.2:

Tunable Photonic Filters using Cascaded All-Pole Micro-rings and All-Zero Interferomers

Le Nguyen Binh

Department of Elctrical and Computer Systems Engineering

Monash University, Wellington Road, Clayton Victoria 3146, Australia

e-mail: le.nguyen.binh@eng.monash.edu.au

Abstract

A digital filter signal processing design method is employed to systematically synthesise tunable photonic filters with variable passband and centre wavelength/frequency characteristics for lowpass, highpass, bandpass and bandstop types. Potential applications of such filters and the existing design techniques in WDM and dispersion equalisation are discussed. Basic optical filter structures, the first-order all-pole photonic filter (FOAPPF) and the first-order all-zero photonic filter (FOAZPF) are described. Thence the design process of tunable optical filters and the design of the second-order Butterworth lowpass, highpass, bandpass and bandstop tunable optical filters are described. The tunabiity of the fiter passband and roll-off band is examined with respect to the pole-zero patten.

1 INTRODUCTION

Tunable photonic filters (PFs) with variable bandwidth and centre frequency characteristics are important in applications where dynamic changes in the bandwidth and centre frequency of the filter are required. One such application is in frequency-division-multiplexing (FDM) or multi- wavelength-division-multiplexed (WDM) optical systems, which utilises the large bandwidth of optical fibres to increase the transmission capacity which is mainly limited by fibre dispersion . In WDM systems, tunable photonic filters are used as optical demultiplexers at the receivers to select one or more desired channels at any wavelength.

There have been reports of several types of tunable PFs such as the optical ring resonators[1], optical transversal filters [2], and Fabry-Perot interferometers [3], [4]. These filters may be referred to as bandpass tunable photonic filters (BPTPF) because their magnitude responses have Gaussian-type characteristics. Another type of tunable PF is the cascaded-coupler Mach-Zehnder channel adding/dropping filter whose output ports constitute a power-complementary pair; one port is used as a bandpass filter while the other port is used as a bandstop filter [5]. It is believed to the best of our knowedge that there has been no previous report of a systematic filter design technique, which can be used to design tunable PFs with the essential features of variable bandwidth and centre frequency characteristics as well as general filtering characteristics such as lowpass, highpass, bandpass and bandstop characteristics.

Micro-rings have been proven to be the most effective resonance structures for optica add/drop muxes, optica fiters etc. Interferometers using planar lightwave circuit technology also gain popularity for integrated photonics. In this report, we present the design of tunable PFs with variable bandwidth and centre frequency characteristics as well as lowpass, highpass, bandpass and bandstop characteristics. We use extensively the structures of micro-ring and integrated interferometers in our proposed photonic filter design. Techniques for the design of digital filters is adopted and described in the Appendix as a reference. The filter design method employing a graphical approach described here is adopted from that proposed by Ngo and Binh [6] in which non-tunable PFs were designed. The all-pole micro-rings and al-zero interferometers of firt order are cascaded and interleaved so as to formulate the z-transform transfer function of the fiters and ease for practica implementation.

The paper is organised as follows. Section 2 outlines the basic structures of tunable filters with much reference to the digital filter design techniques given in the Appendix. The composite design of optical filters whose filtered band and centre optical frquency are tunable to a desired position is described illustrating the effective ness of the systematic design procedures.

2 BASIC STRUCTURES OF TUNABLE PHOTONIC FILTERS

This section describes the basic filter structures, namely, the first-order all-pole photonic filter (FOAPPF) and the first-order all-zero photonic filter (FOAZPF) of tunable PFs. These filters employ a fundamnetal approach of recursive filters whose characteristics are summarised in the Appendix.

2.1 First-Order All-Pole PF

Considering a basic optical filter structure shown in *Figure 1* represents the *k*th-stage of a FOAPPF[1] using the planar lightwave circuit (PLC) technology. The FOAPPF consists of an optical waveguide loop interconnected by two identical tunable couplers (TCs) and a thermo-optic phase shifter (PS). This is the basic structures of mcro-ring resonators. The TC, which is a symmetrical Mach-Zehnder interferometer, consists of, in this case, two 3-dB directional couplers interconnected by two waveguide arms of equal length. This structure can be implemented using the planar lightwave circuit (PLC) silica on siicon for the 1550 nm waveength region. The phase shifter is usually implemented by thermooptic effect using an electrode coated on the surace of the micro-ring. One can consider that thethe input port is the ADD port and the output port is the DROP port of ADD/DROPPmuxes currently popular in metropolitan optica networks. Thence we can observe in later section that when these PFs are cascacded the would for severa dropp and add ports.

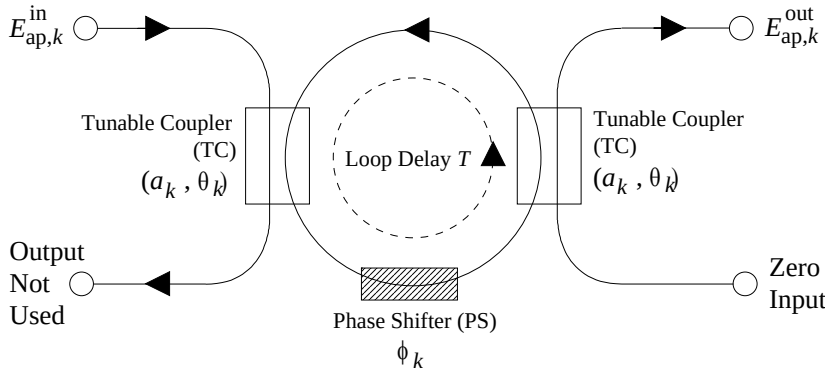

Figure 1 Schematic diagram of the kth-stage first-order all-pole optical filter (FOAPPF) using the PLC technology.

The TC has the

$$\text{complex cross-coupled coefficient} = \sqrt{\gamma_{\mathrm{w}} a_k}\,\exp(j\theta_k) \tag{1}$$

and

$$\text{complex direct-coupled coefficient} = \sqrt{\gamma_{\mathrm{w}}(1-a_k)}\,\exp(j\theta_k) \tag{2}$$

where γ_{w} (typically $\gamma_{\mathrm{w}} = 0.89$ for an insertion loss of 0.5 dB) is the intensity transmission coefficient of the TC. The cross-coupled intensity coefficient of the TC is given as

$$a_k = (1+\cos\varphi_k)/2\,, \qquad (0 \le a_k \le 1) \tag{3}$$

from which the phase shift of the PS on the upper arm of the TC is given by

$$\varphi_k = \cos^{-1}(2a_k - 1) \qquad (0 \le \varphi_k \le 2\pi) \tag{4}$$

and the resulting phase shift of the TC is given as

[1]Note that the FOAPPF has been used in the design and implementation of an optical integrator for dark-soliton generation

$$\theta_k = \tan^{-1}\left[\frac{\sin\varphi_k}{\cos\varphi_k - 1}\right] \qquad (-\pi/2 \le \theta_k \le \pi/2). \tag{5}$$

The optical transmittances of the upper (Λ_{1k}) and lower (Λ_{2k}) halves of the waveguide ring are defined as

$$\Lambda_{1k} = \exp(-\alpha_w L_{1k})\exp(-j\omega T_{1k}) \tag{6}$$

$$\Lambda_{2k} = \exp(-\alpha_w L_{2k})\exp(-j\omega T_{2k})\exp(j\phi_k) \tag{7}$$

where the amplitude waveguide propagation loss is typically $\alpha_w = 0.01151\ \text{cm}^{-1}$ as determined from $\alpha_w = \alpha_w(\text{dB/cm})/8.686$ with $\alpha_w(\text{dB/cm}) = 0.1\ \text{dB/cm}$, L_{1k} and L_{2k} are the waveguide lengths of the upper and lower halves of the micro-ring T_{1k} and T_{2k} are the corresponding time delays of the upper and lower halves of the ring, $j = \sqrt{-1}$, ω is the angular optical frequency, and ϕ_k $(0 \le \phi_k \le 2\pi)$ is the phase shift of the PS. Note that the lengths of the lower and upper halves of the ring do not necessarily need to be the same.

Using the signal-flow graph method described in Ref.[6] together with eqns. (A1) and (A2), the transfer function of the *k*th-stage FOAPPF is simply given, by inspection of *Figure 1*, as

$$H_{\text{ap},k}(\omega) = \frac{E_{\text{ap},k}^{\text{out}}}{E_{\text{ap},k}^{\text{in}}} = \frac{\gamma_w a_k \exp(j2\theta_k)\Lambda_{2k}}{1 - \gamma_w(1-a_k)\exp(j2\theta_k)\Lambda_{1k}\Lambda_{2k}} \tag{8}$$

where $E_{\text{ap},k}^{\text{in}}$ and $E_{\text{ap},k}^{\text{out}}$ are the electric-field amplitudes at the input and output ports of the FOAPPF, respectively. It is useful to define the waveguide loop length L, the waveguide loop delay *T*, and the *z*-transform parameter as

$$L = L_{1k} + L_{2k} \tag{9}$$

$$T = T_{1k} + T_{2k} \tag{10}$$

$$z = \exp(j\omega T) \tag{11}$$

Substituting Eqs. (6), (7) and (9)–(11) into Eq. (8), the *z*-transform transfer function of the *k*th-stage FOAPPF becomes

$$H_{\text{ap},k}(z) = \frac{A_{\text{ap},k}\exp\left(j(2\theta_k + \phi_k)\right)\exp(-j\omega T_{2k})z}{z - p_k} \tag{12}$$

where the amplitude $A_{\text{ap},k}$ and the pole location p_k in the *z*-plane are given by

$$A_{\text{ap},k} = \gamma_w a_k \exp(-\alpha_w L_{2k}), \tag{13}$$

$$p_k = \gamma_w(1-a_k)\exp(-\alpha_w L)\exp\left(j(2\theta_k + \phi_k)\right). \tag{14}$$

It is useful to express Eq. (14) in the phasor form as

$$p_k = |p_k| \exp(j \arg(p_k)) \qquad (0 \le |p_k| < 1), \tag{15}$$

where
$$|p_k| = \gamma_w (1 - a_k) \exp(-\alpha_w L) \tag{16}$$

$$\arg(p_k) = 2\theta_k + \phi_k. \tag{17}$$

2.2 First-Order All-Zero Optical Filter

Figure 2 shows the schematic diagram of the *k*th-stage FOAZPF[2] using the PLC technology. The FOAZPF, which is an asymmetrical Mach-Zehnder interferometer, consists of two waveguide directional couplers DC1 and DC2, with cross-coupled intensity coefficients b_{1k} and b_{2k} $(0 \le b_{1k}, b_{2k} \le 1)$, respectively, which are interconnected by two unequal waveguide arms with a differential time delay of *T*. The PS on the lower arm has a phase shift of ψ_k $(0 \le \psi_k \le 2\pi)$.

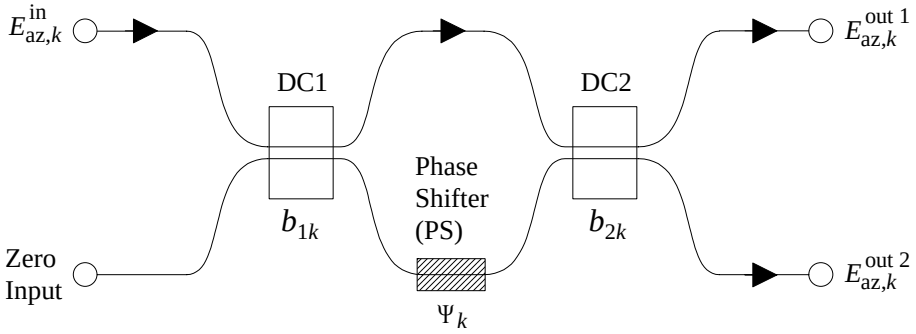

Figure 2 Schematic diagram of the kth-stage first-order all-zero optical filter (FOAZPF) using the PLC technology.

The optical transmittances of the upper (Λ_{3k}) and lower (Λ_{4k}) waveguide arms are defined as

$$\Lambda_{3k} = \exp(-\alpha_w L_{3k}) \exp(-j\omega T_{3k}) \tag{18}$$

$$\Lambda_{4k} = \exp(-\alpha_w L_{4k}) \exp(-j\omega T_{4k}) \exp(j\psi_k) \tag{19}$$

where L_{3k} and L_{4k} are the waveguide lengths of the upper and lower arms, and T_{3k} and T_{4k} are the corresponding time delays of the upper and lower arms.

Using the signal-flow graph method as described in Ref.[6] , the transfer function of the *k*th-stage FOAZPF (for the upper output port) is simply given, by inspection of *Figure 2*, as

$$H_{az,k}(\omega) = \frac{E_{az,k}^{out\ 1}}{E_{az,k}^{in}} = \sqrt{\gamma_{az}(1 - b_{1k})(1 - b_{2k})}\Lambda_{3k} - \sqrt{\gamma_{az} b_{1k} b_{2k}}\Lambda_{4k} \tag{20}$$

[2]Note that the FOAZOF has been used as the optical dark-soliton detectors

where $E_{\mathrm{az},k}^{\mathrm{in}}$ and $E_{\mathrm{az},k}^{\mathrm{out}\,1}$ and $E_{\mathrm{az},k}^{\mathrm{out}\,2}$ describe the electric-field amplitudes at the input and output ports of the FOAZPF, respectively, and γ_{az} (which is assumed to be $\gamma_{\mathrm{az}} = \gamma_{\mathrm{w}} = 0.89$ (a typical value) for analytical simplicity) is the intensity transmission coefficient of the FOAZPF. It is useful to define the differential length[3] L and the differential time delay[4] T as

$$L = L_{4k} - L_{3k} \tag{21}$$

$$T = T_{4k} - T_{3k} \tag{22}$$

By substituting Eqs. (18), (19), (20), (22) and (11) into Eq. (21), the *z*-transform transfer function of the *k*th-stage FOAZPF (for the upper output port) becomes

$$H_{\mathrm{az},k}(z) = A_{\mathrm{az},k} \exp(-j\omega T_{3k}) z^{-1}(z - z_k) \tag{23}$$

where the amplitude $A_{\mathrm{az},k}$ and the zero location z_k in the *z*-plane are given by

$$A_{\mathrm{az},k} = \sqrt{\gamma_{\mathrm{az}}(1-b_{1k})(1-b_{2k})}\exp(-\alpha_{\mathrm{w}} L_{3k}) \tag{24}$$

$$z_k = \sqrt{\frac{b_{1k}b_{2k}}{(1-b_{1k})(1-b_{2k})}}\exp(-\alpha_{\mathrm{w}} L)\exp(j\psi_k) \tag{25}$$

It is useful to express Eq. (25) in the phasor form as

$$z_k = |z_k|\exp\big(j\arg(z_k)\big) \tag{26}$$

where $|z_k| = \sqrt{\frac{b_{1k}b_{2k}}{(1-b_{1k})(1-b_{2k})}}\exp(-\alpha_{\mathrm{w}} L)$ (27)

$$\arg(z_k) = \psi_k \tag{28}$$

Similarly, the *z*-transform transfer function of the *k*th-stage FOAZPF (for the lower output port) is given by

$$H_{\mathrm{az},k}^{*}(z) = \frac{E_{\mathrm{az},k}^{\mathrm{out}\,2}}{E_{\mathrm{az},k}^{\mathrm{in}}} = A_{\mathrm{az},k}^{*}\exp\big(-j(\omega T_{3k} + \pi/2)\big) z^{-1}(z - z_k^{*}) \tag{29}$$

where the amplitude $A_{\mathrm{az},k}^{*}$ and the zero location z_k^{*} in the *z*-plane are given by

$$A_{\mathrm{az},k}^{*} = \sqrt{\gamma_{\mathrm{az}} b_{2k}(1-b_{1k})}\exp(-\alpha_{\mathrm{w}} L_{3k}) \tag{30}$$

$$z_k^{*} = \sqrt{\frac{b_{1k}(1-b_{2k})}{b_{2k}(1-b_{1k})}}\exp(-\alpha_{\mathrm{w}} L)\exp\big(j(\psi_k + \pi)\big) \tag{31}$$

---

[3] L is the differential length of the *k*th-stage FOAZOF [see Eq. (21)] as well as the loop length of the *k*th-stage FOAPPF [see Eq. (9)].

[4] T is the differential time delay of the *k*th-stage FOAZOF [see Eq. (22)] as well as the loop delay of the *k*th-stage FOAPPF [see Eq. (10)].

In the phasor form, Eq. (31) becomes

$$z_k^* = \left|z_k^*\right| \exp\left(j\arg(z_k^*)\right) \tag{32}$$

where $$\left|z_k^*\right| = \sqrt{\frac{b_{1k}(1-b_{2k})}{b_{2k}(1-b_{1k})}} \exp(-\alpha_w L) \tag{33}$$

$$\arg(z_k^*) = \psi_k + \pi \tag{34}$$

From Eqs. (28) and (34), the zero z_k (for the upper output port) is out of phase with the zero z_k^* (for the lower output port) by π. This means that the transfer functions $H_{\text{az},k}(z)$ and $H_{\text{az},k}^*(z)$ constitute a power-complementary pair:

$$\left|H_{\text{az},k}(z)\right|^2 + \left|H_{\text{az},k}^*(z)\right|^2 = 1 \tag{35}$$

In other words, if $H_{\text{az},k}(z)$ has a lowpass magnitude response then $H_{\text{az},k}^*(z)$ has a highpass magnitude response, an important property which is useful in the design of tunable optical filters.

Note that only the transfer function $H_{\text{az},k}(z)$ is used in the design of tunable optical filters as described in the following section.

2.3 *M*th-Order Tunable Optical Filter

The transfer function of the *M*th-order tunable all-pole optical filter, which is the transfer function of the cascade of *M* FOAPPFs, is defined as

$$H_{\text{ap}}(z) = \prod_{k=1}^{M} H_{\text{ap},k}(z) \tag{36}$$

The transfer function of the *M*th-order tunable all-zero optical filter, which is the transfer function of the cascade of *M* FOAZPFs, is defined as

$$H_{\text{az}}(z) = \prod_{k=1}^{M} H_{\text{az},k}(z) \tag{37}$$

The transfer function of the *M*th-order tunable optical filter can thus be written as

$$H(z) = G \cdot H_{\text{ap}}(z) \cdot H_{\text{az}}(z) \tag{38}$$

where *G* is the amplitude optical gain of the erbium-doped fibre amplifier (EDFA).

Figure 3 shows the block diagram representation of Eq. (38) which describes the transfer function between the input port and the upper output port (i.e., Output 1). The lower output port (Output 2) is not used in filter design but its usefulness will be investigated.

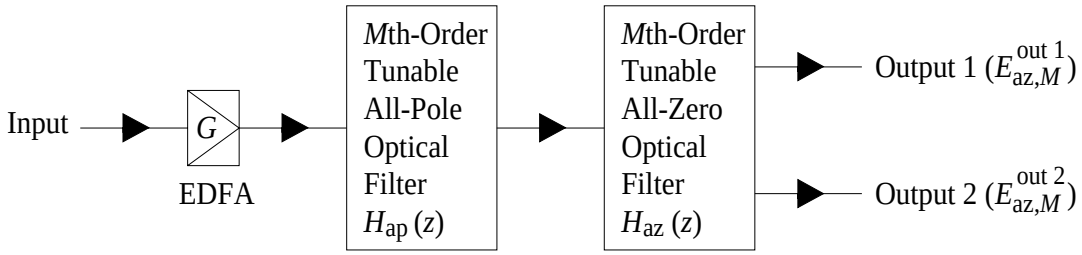

Figure 3 Block diagram representation of the Mth-order tunable PF – all- pole and all-zero interleaved.

Substituting Eqs. (12), (23), (36) and (37) into Eq. (38), the transfer function of the *M*th-order tunable optical filter is given by

$$H(z) = \exp\left[j\left(\sum_{k=1}^{M} (2\theta_k + \phi_k) - \omega \sum_{k=1}^{M} (T_{2k} + T_{3k}) \right) \right] \cdot \left[A \prod_{k=1}^{M} \frac{(z - z_k)}{(z - p_k)} \right] \tag{39}$$

where the amplitude *A* is defined as

$$A = G \prod_{k=1}^{M} A_{\mathrm{ap},k} A_{\mathrm{az},k} \tag{40}$$

The proposed *M*th-order tunable optical filter has the advantage that its poles and zeros can be adjusted independently of each other. Thus, a particular pole-zero pattern can easily be obtained to design filters with general characteristics.

3 DESIGN OF TUNABLE PHOTONIC FILTERS

This section describes the design of tunable optical filters and also presents a detailed design of the second-order Butterworth lowpass, highpass, bandpass and bandstop tunable PFs with variable 3dB bandwidth and centre frequency characteristics.

In general, the design of a tunable optical filter from the characteristics of a digital filter involves the following stages: (1) the specification of the desired magnitude response of the optical filter in the optical domain, which is usually described by the spectrum of the optical signals to be processed by the filter; (2) the design of a digital filter whose magnitude response in the digital domain approximates the desired magnitude response of the optical filter in the optical domain; (3) the design of the PF structure whose transfer function is similar in form to the transfer function of the digital filter; (4) the design of the parameters of the optical filter structure using the pole-zero characteristics of the digital filter; and (5) the practical realisation of the PF.

3.1 Design Equations for Tunable Optical Filters

For analytical simplicity, the exponential factor in Eq. (47), which represents a linear phase term, is neglected because it has no effect on the magnitude response of the filter. The design of a tunable optical filter from the characteristics of a digital filter requires the second factor of Eq. (47) to be equal to Eq. (1) such that the following equations hold:

$$A = \hat{A} \tag{41}$$

$$p_k = \hat{p}_k \tag{42}$$

$$z_k = \hat{z}_k \tag{43}$$

Substituting Eqs. (13), (24) and (40) into Eq. (41) results in

$$G = \frac{\left(\gamma_{\mathrm{w}} \gamma_{\mathrm{az}}^{1/2}\right)^{-M} \hat{A}}{\prod_{k=1}^{M} a_k \left[(1-b_{1k})(1-b_{2k})\right]^{1/2} \exp\left(-\alpha_{\mathrm{w}} (L_{2k} + L_{3k})\right)} \tag{44}$$

Using Eqs. (A2) and (15)–(18) and subsituting into Eq. (42) results in

$$a_k = 1 - \frac{|\hat{p}_k|}{\gamma_{\mathrm{w}} \exp(-\alpha_{\mathrm{w}} L)} \quad \text{with} \quad |\hat{p}_k| \le \gamma_{\mathrm{w}} \exp(-\alpha_{\mathrm{w}} L) \tag{45}$$

$$\phi_k = \begin{cases} \arg(\hat{p}_k) - 2\theta_k, & \arg(\hat{p}_k) - 2\theta_k \ge 0, \\ \arg(\hat{p}_k) - 2\theta_k + 2\pi, & \arg(\hat{p}_k) - 2\theta_k < 0. \end{cases} \tag{46}$$

From Eq. (45), the largest value of the filter pole (i.e., $|\hat{p}_k|$) is restricted by the loss of the waveguide loop [i.e., $\gamma_{\mathrm{w}} \exp(-\alpha_{\mathrm{w}} L)$]. For practical purposes, a full cycle phase shift of 2π has been added, without affecting the filter performance, to the second equation of Eq. (46) so that ϕ_k takes a positive value (i.e., $0 \le \phi_k \le 2\pi$). Substituting Eqs. (A3) and (26)–(28) into Eq. (43) and using the relation $|z_k| = |z_k^*| = |\hat{z}_k| = 1$ (i.e., the zeros are located exactly on the unit circle) results in

$$b_{1k} = \frac{1}{1 + \exp(-2\alpha_{\mathrm{w}} L)} \tag{47}$$

$$b_{2k} = 1/2 \tag{48}$$

$$\psi_k = \begin{cases} \arg(\hat{z}_k), & \arg(\hat{z}_k) \ge 0, \\ \arg(\hat{z}_k) + 2\pi, & \arg(\hat{z}_k) < 0. \end{cases} \tag{49}$$

To change the centre frequency of the tunable optical filter without affecting its bandwidth, an additional phase shift of δ_0 $(0 < \delta_0 < 2\pi)$ must be added to Eqs. (46) and (49), resulting in

$$\phi_k = \begin{cases} \arg(\hat{p}_k) - 2\theta_k + \delta_0, & \arg(\hat{p}_k) - 2\theta_k + \delta_0 \ge 0, \\ \arg(\hat{p}_k) - 2\theta_k + \delta_0 + 2\pi, & \arg(\hat{p}_k) - 2\theta_k + \delta_0 < 0. \end{cases} \tag{50}$$

$$\psi_k = \begin{cases} \arg(\hat{z}_k) + \delta_0, & \arg(\hat{z}_k) + \delta_0 \ge 0 \\ \arg(\hat{z}_k) + \delta_0 + 2\pi, & \arg(\hat{z}_k) + \delta_0 < 0 \end{cases} \tag{51}$$

In summary, the design equations for the design of tunable optical filters are Eqs. (4), (5), (44), (45), (47), (48), (50) and (51).

3.2 Second-Order Butterworth Tunable PFs

To demonstrate the effectiveness of the proposed filter design technique, this section describes the design of the second-order (M=2) Butterworth lowpass, highpass, bandpass and bandstop tunable PFs with variable bandwidth and centre frequency characteristics.

In this example, a $1/T = 5$ GHz filter is considered, resulting in $T = 200$ ps and $L = 4$ cm. Using $\gamma_{\mathrm{w}} = \gamma_{\mathrm{az}} = 0.89$, $\alpha_{\mathrm{w}} = 0.01151\ \mathrm{cm}^{-1}$ and hence $\exp(-\alpha_{\mathrm{w}} L) = 0.955$, Eqs. (45) and (47) become

$$a_k = 1 - 1.18|\hat{p}_k| \qquad |\hat{p}_k| \le 0.85 \tag{52}$$

$$b_{1k} = 0.523 \tag{53}$$

the corresponding gain coefficient is

$$G = \frac{(0.392)^{-M}\hat{A}}{\prod_{k=1}^{M} a_k} \tag{54}$$

where $\exp\left(-\alpha_{\mathrm{w}}(L_{2k} + L_{3k})\right) = \exp(-\alpha_{\mathrm{w}} L) = 0.955$ has been assumed for numerical simplicity. In summary, Eqs. (4), (5), (48) and (50)–(54) are used in the design of the second-order Butterworth tunable PFs. The following definitions are used hereafter. The normalised photonic frequency on the frequency axis of the squared magnitude response represents $\omega T/\pi$, the squared magnitude responses are plotted over the Nyquist interval (i.e., $0 \le \omega T/\pi \le 1$), ω_{c} is the 3-dB angular cutoff frequency of the lowpass and highpass filters, and ω_{c1} (ω_{c2}) is the 3-dB angular lower (upper) corner frequency of the bandpass and bandstop filters where $\omega_{\mathrm{c1}} < \omega_{\mathrm{c2}}$. For the lowpass and highpass filters, the normalised 3-dB bandwidth is defined as $\omega_{\mathrm{c}} T/\pi$. For the bandpass and bandstop filters, the normalised 3-dB bandwidth is defined as $(\omega_{\mathrm{c2}} - \omega_{\mathrm{c1}})T/\pi$.

Using MATLAB, *Table 1* and *Table 2* show the computed design parameters of the second-order Butterworth lowpass and highpass (*Table 1*) digital filters with various cutoff frequencies and bandpass and bandstop (*Table 2*) digital filters[5] with various sets of lower and upper corner frequencies. Using Eqs. (4), (5), (48) and (50)–(54), *Table 3* and *Table 4* show the computed design parameters of the second-order Butterworth lowpass and highpass (*Table 3*) and bandpass and bandstop (*Table 4*) tunable PFs with variable bandwidth and fixed centre frequency (i.e., $\delta_0 = 0$) characteristics.

Figure 4 shows the characteristics of the tuning parameters versus the normalised bandwidth (i.e., $\omega_{\mathrm{c}} T/\pi$) of the lowpass and highpass tunable PFs with variable bandwidth (i.e., $0.1 \le \omega_{\mathrm{c}} T/\pi \le 0.9$)

[5]These digital filters are described by the transfer function given in Eq. (1).

and fixed centre frequency (i.e., $\delta_0 = 0$) characteristics. The values of these parameters are obtained from *Table 3*.

			Poles of $\hat{H}_{\text{ap},k}(z)$ $(k=1,2)$			Zeros of $\hat{H}_{\text{az},k}(z)$ $k=1,2$	
Filter Type	ω_c	$\hat{A}$	$\lvert\hat{p}_1\rvert = \lvert\hat{p}$	$\arg(\hat{p}_1)$	$\arg(\hat{p}_2) = -\arg(\hat{p}_1)$	$\lvert\hat{z}_1\rvert = \lvert\hat{z}_2\rvert$	$\arg(\hat{z}_1) = \arg(\hat{z}_2)$
Lowpass	0.1	0.0201	0.8008	–0.2258	0.2258	1	π
	0.2	0.0675	0.6425	–0.4746	0.4746	1	π
	0.3	0.1311	0.5217	–0.7718	0.7718	1	π
	0.4	0.2066	0.4425	–1.1401	1.1401	1	π
	0.5	0.2929	0.4142	–1.5708	1.5708	1	π
	0.6	0.3913	0.4425	–2.0015	2.0015	1	π
	0.7	0.5050	0.5217	–2.3698	2.3698	1	π
	0.8	0.6389	0.6425	–2.6670	2.6670	1	π
	0.9	0.8006	0.8008	–2.9158	2.9158	1	π
Highpass	0.1	0.8006	0.8008	–0.2258	0.2258	1	0
	0.2	0.6389	0.6425	–0.4746	0.4746	1	0
	0.3	0.5050	0.5217	–0.7718	0.7718	1	0
	0.4	0.3913	0.4425	–1.1401	1.1401	1	0
	0.5	0.2929	0.4142	–1.5708	1.5708	1	0
	0.6	0.2066	0.4425	–2.0015	2.0015	1	0
	0.7	0.1311	0.5217	–2.3698	2.3698	1	0
	0.8	0.0675	0.6425	–2.6670	2.6670	1	0
	0.9	0.0201	0.8008	–2.9158	2.9158	1	0

Table 1 Design parameters of the second-order (M=2) Butterworth lowpass and highpass digital filters with various cutoff frequencies. For each bandwidth $\omega_c T/\pi$, both the lowpass and highpass filters have the same poles which occur in complex-conjugate pairs. The zeros are located exactly on the unit circle in the z-plane but there is a phase difference of π between the zeros of the lowpass and highpass filters.

				Poles of $\hat{H}_{\text{ap},k}(z)$, $(k=1,2)$			Zeros of $\hat{H}_{\text{az},k}(z)$, $(k=1,2)$		
Filter Type	$\omega_{c1}T/\pi$	$\omega_{c2}T/\pi$	$\hat{A}$	$\lvert\hat{p}_1\rvert =$	$\arg(\hat{p}_1)$	$\arg(\hat{p}_2)$	$\lvert\hat{z}_1\rvert =$	$\arg(\hat{z}_1)$	$\arg(\hat{z}_2)$
Bandpass	0.40 0.35 0.30 0.25 0.20 0.15 0.10	0.60 0.65 0.70 0.75 0.80 0.85 0.90	0.2425 0.3375 0.4208 0.5000 0.5792 0.6625 0.7548	0.7138 0.5700 0.3980 0 0.3980 0.5700 0.7138	$-\pi/2$ $-\pi/2$ $-\pi/2$ 0 π π π	$\pi/2$ $\pi/2$ $\pi/2$ 0 0 0 0	1 1 1 1 1 1 1	0 0 0 0 0 0 0	π π π π π π π
Bandstop	0.40 0.35 0.30 0.25 0.20 0.15 0.10	0.60 0.65 0.70 0.75 0.80 0.85 0.90	0.7548 0.6625 0.5792 0.5000 0.4208 0.3375 0.2425	0.7138 0.5700 0.3980 0 0.3980 0.5700 0.7138	$-\pi/2$ $-\pi/2$ $-\pi/2$ 0 π π π	$\pi/2$ $\pi/2$ $\pi/2$ 0 0 0 0	1 1 1 1 1 1 1	$-\pi/2$ $-\pi/2$ $-\pi/2$ $-\pi/2$ $-\pi/2$ $-\pi/2$ $-\pi/2$	$\pi/2$ $\pi/2$ $\pi/2$ $\pi/2$ $\pi/2$ $\pi/2$ $\pi/2$

Table 2 Design parameters of the second-order (M=2) Butterworth bandpass and bandstop digital filters with various sets of lower ($\omega_{c1}T/\pi$) and upper ($\omega_{c2}T/\pi$) corner frequencies. For each set of corner frequencies, both the bandpass and bandstop filters have the same poles which occur in complex-conjugate pairs. The zeros are located exactly on the unit circle in the z-plane.

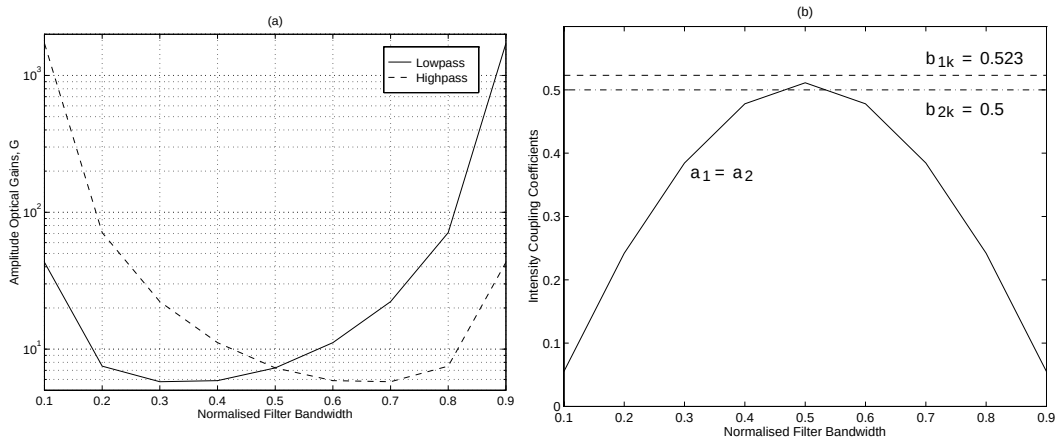

(a) (b)

Figure 4 Characteristics of the tuning parameters versus the normalised bandwidth of the lowpass and highpass tunable PFs with variable bandwidth and fixed centre frequency (i.e., $\delta_0 = 0$) characteristic. (a) EDFA amplitude gains, G. (b) Intensity coupling coefficients of both the lowpass and highpass filters.

			Parameters of $H_{\mathrm{ap},k}(z)$ $(k=1,2)$					Parameters of $H_{\mathrm{az},k}(z)$ $(k=1,2)$		
Filter Type	$\omega_c T$	G	$a_1 = a_2$	$\varphi_1 = \varphi_2$	$\theta_1 = \theta_2$	ϕ_1	ϕ_2	b_{1k}	b_{2k}	$\psi_1 = \psi_2$
Lowpass	0.1	43.08	0.0551	2.6677	–0.2369	0.2480	0.6996	0.5230	0.5000	π
	0.2	7.507	0.2419	2.1132	–0.5142	0.5538	1.5030	0.5230	0.5000	π
	0.3	5.774	0.3844	1.8041	–0.6687	0.5656	2.1092	0.5230	0.5000	π
	0.4	5.887	0.4779	1.6150	–0.7633	0.3865	2.6667	0.5230	0.5000	π
	0.5	7.294	0.5112	1.5484	–0.7966	0.0224	3.1640	0.5230	0.5000	π
	0.6	11.15	0.4779	1.6150	–0.7633	5.8083	3.5281	0.5230	0.5000	π
	0.7	22.24	0.3844	1.8041	–0.6687	5.2508	3.7072	0.5230	0.5000	π
	0.8	71.05	0.2419	2.1132	–0.5142	4.6446	3.6954	0.5230	0.5000	π
	0.9	1716	0.0551	2.6677	–0.2369	3.8412	3.3896	0.5230	0.5000	π
Highpass	0.1	1716	0.0551	2.6677	–0.2369	0.2480	0.6996	0.5230	0.5000	0
	0.2	71.05	0.2419	2.1132	–0.5142	0.5538	1.5030	0.5230	0.5000	0
	0.3	22.24	0.3844	1.8041	–0.6687	0.5656	2.1092	0.5230	0.5000	0
	0.4	11.15	0.4779	1.6150	–0.7633	0.3865	2.6667	0.5230	0.5000	0
	0.5	7.294	0.5112	1.5484	–0.7966	0.0224	3.1640	0.5230	0.5000	0
	0.6	5.887	0.4779	1.6150	–0.7633	5.8083	3.5281	0.5230	0.5000	0
	0.7	5.774	0.3844	1.8041	–0.6687	5.2508	3.7072	0.5230	0.5000	0
	0.8	7.507	0.2419	2.1132	–0.5142	4.6446	3.6954	0.5230	0.5000	0
	0.9	43.08	0.0551	2.6677	–0.2369	3.8412	3.3896	0.5230	0.5000	0

Table 3 Design parameters of the second-order ($M = 2$) Butterworth lowpass and highpass tunable PFs with variable bandwidth and fixed centre frequency (i.e., $\delta_0 = 0$) characteristics. The values of these parameters are obtained from Eqs. (12), (13), (56) and (58)–(62) and Table 1. For each bandwidth $\omega_c T/\pi$, both the lowpass and highpass filters have the same poles and hence the same parameters of the FOAPPFs, that is, the same coupling coefficients (i.e., a_1 and a_2) and the same phase shifts (i.e., φ_1, φ_2, ϕ_1 and ϕ_2). For each bandwidth $\omega_c T/\pi$, there is a phase difference of π between the FOAZPFs of the lowpass and highpass filters.

3.3 Tuning Parameters of the Lowpass and Highpass Tunable PFs

The gain curves in *Figure 4*(a) show that a large EDFA gain, which can be achieved by having two EDFAs in cascade, is required for a very small or large filter bandwidth (e.g., $G = 1716$ or 65 dB is required at $\omega_c T/\pi = 0.1$ for the highpass filter and at $\omega_c T/\pi = 0.9$ for the lowpass filter). These curves are symmetrical about the mid-band frequency (i.e., the required gain at $\omega_c T/\pi$ for the lowpass filter is the same as that at $1-\omega_c T/\pi$ for the highpass filter). *Figure 4*(b) shows the intensity coupling coefficients of the FOAPPFs (i.e., $a_1 = a_2$) and FOAZPFs (i.e., $b_{1k} = 0.523$ and $b_{2k} = 0.5$) for both the lowpass and highpass filters. The required coupling coefficients $a_1 = a_2$ can be obtained by varying the phase shifts $\varphi_1 = \varphi_2$ of the TCs. Note that both the curves of $a_1 = a_2$ and $\varphi_1 = \varphi_2$ are symmetrical about the mid-band frequency. The lowpass and highpass filters require the phase shifts $\psi_1 = \psi_2 = \pi$ and $\psi_1 = \psi_2 = 0$ respectively, of the FOAZPFs.

3.4 Tuning Parameters of Bandpass and Bandstop Tunable PFs

Figure 5 shows the characteristics of the tuning parameters versus the normalised bandwidth (i.e., $(\omega_{c2} - \omega_{c1})T/\pi$) of the bandpass and bandstop tunable PFs with variable bandwidth (i.e., $0.2 \le (\omega_{c2} - \omega_{c1})T/\pi \le 0.8$) and fixed centre frequency (i.e., $\delta_0 = 0$) characteristics. The values of these parameters are obtained from *Table 4*.

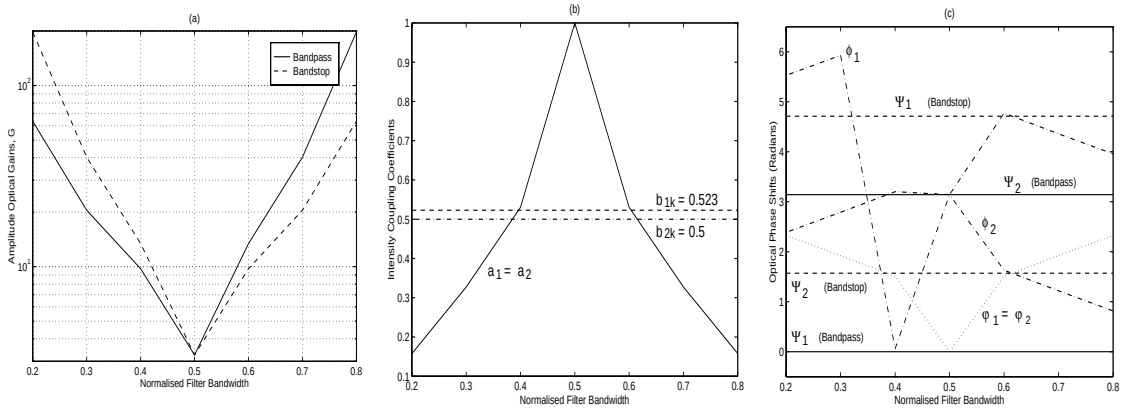

(a) (b) (c)

Figure 5 Characteristics of the tuning parameters versus the normalised bandwidth of the bandpass and bandstop tunable PFs with variable bandwidth and fixed centre frequency (i.e., $\delta_0 = 0$) characteristics (a) EDFA amplitude gains, G. (b) Intensity coupling coefficients of both the bandpass and bandstop filters. (c) Optical phase shifts, where ϕ_1, ϕ_2 and $\varphi_1 = \varphi_2$ are the phase shifts of both the bandpass and bandstop filters.

				Parameters of $H_{\mathrm{ap},k}(z)$, $(k=1,2)$				Parameters of $H_{\mathrm{az},k}(z)$, $(k=1,2)$				
Filter Type	$\omega_{c1}T$	$\omega_{c2}T$	G	$a_1=a_2$	$\varphi_1=\varphi_2$	$\theta_1=\theta_2$	ϕ_1	ϕ_2	b_{1k}	b_{2k}	ψ_1	ψ_2
Bandpass	0.40	0.60	63.46	0.1577	2.3249	–0.4083	5.5290	2.3874	0.5230	0.5000	0	π
	0.35	0.65	20.49	0.3274	1.9232	–0.6092	5.9308	2.7892	0.5230	0.5000	0	π
	0.30	0.70	9.734	0.5304	1.5100	–0.8158	0.0608	3.2024	0.5230	0.5000	0	π
	0.25	0.75	3.254	1.0000	0	–1.5708	3.1416	3.1416	0.5230	0.5000	0	π
	0.20	0.80	13.40	0.5304	1.5100	–0.8158	4.7732	1.6316	0.5230	0.5000	0	π
	0.15	0.85	40.22	0.3274	1.9232	–0.6092	4.3600	1.2184	0.5230	0.5000	0	π
	0.10	0.90	197.5	0.1577	2.3249	–0.4083	3.9582	0.8166	0.5230	0.5000	0	π
Bandstop	0.40	0.60	197.5	0.1577	2.3249	–0.4083	5.5290	2.3874	0.5230	0.5000	3π	$\pi/2$
	0.35	0.65	40.22	0.3274	1.9232	–0.6092	5.9308	2.7892	0.5230	0.5000	3π	$\pi/2$
	0.30	0.70	13.40	0.5304	1.5100	–0.8158	0.0608	3.2024	0.5230	0.5000	3π	$\pi/2$
	0.25	0.75	3.254	1.0000	0	–1.5708	3.1416	3.1416	0.5230	0.5000	3π	$\pi/2$
	0.20	0.80	9.734	0.5304	1.5100	–0.8158	4.7732	1.6316	0.5230	0.5000	3π	$\pi/2$
	0.15	0.85	20.49	0.3274	1.9232	–0.6092	4.3600	1.2184	0.5230	0.5000	3π	$\pi/2$
	0.10	0.90	63.46	0.1577	2.3249	–0.4083	3.9582	0.8166	0.5230	0.5000	3π	$\pi/2$

Table 4 Design parameters of the second-order (M=2) Butterworth bandpass and bandstop tunable PFs with variable bandwidth and fixed centre frequency (i.e., $\delta_0=0$) characteristics. The values of these parameters are obtained from Eqs. (12), (13), (56) and (58)–(62) and Table 2. For each bandwidth $(\omega_{c2}-\omega_{c1})T/\pi$, both the bandpass and bandstop filters have the same poles and hence the same parameters of the FOAPPFs, that is, the same coupling coefficients (i.e., a_1 and a_2) and the same phase shifts (i.e., φ_1, φ_2, ϕ_1 and ϕ_2).

The gain curves in *Figure 5*(a) show that a large EDFA gain is required for a very small or large filter bandwidth (e.g., $G=197.5$ or 46 dB is required at $(\omega_{c2}-\omega_{c1})T/\pi=0.2$ for the bandstop filter and at $(\omega_{c2}-\omega_{c1})T/\pi=0.8$ for the bandpass filter). These curves are symmetrical about the mid-band frequency (i.e., the required gain at $(\omega_{c2}-\omega_{c1})T/\pi$ for the bandpass filter is the same as that at $1-(\omega_{c2}-\omega_{c1})T/\pi$ for the bandstop filter). *Figure 5*(b) shows the intensity coupling coefficients of the FOAPPFs (i.e., $a_1=a_2$) and FOAZPFs (i.e., $b_{1k}=0.523$ and $b_{2k}=0.5$) for both the bandpass and bandstop filters. The required coupling coefficients $a_1=a_2$ can be obtained by varying the phase shifts $\varphi_1=\varphi_2$ of the TCs [see the dotted-dotted curve in *Figure 5*(c)]. Note that both the curves of $a_1=a_2$ and $\varphi_1=\varphi_2$ are symmetrical about the mid-band frequency (i.e., the required values at $(\omega_{c2}-\omega_{c1})T/\pi$ are the same as those at $1-(\omega_{c2}-\omega_{c1})T/\pi$). The dotted-dashed curves in *Figure 5*(c) show the required phase shifts ϕ_1 and ϕ_2 of the FOAPPFs for both the bandpass and bandstop filters. The bandpass and bandstop filters require the phase shifts $(\psi_1=0,\psi_2=\pi)$ (see the solid curves) and $(\psi_1=3\pi/2,\psi_2=\pi/2)$ (see the dashed-dashed curves), respectively, of the FOAZPFs.

3.5 Summary of Tuning Parameters of Micro-Ring PFs

The tunable PFs with lowpass, highpass, bandpass and bandstop characteristics can be summarised as: (i) For a particular filter bandwidth, the phase shifts (ψ_1,ψ_2) of the FOAZPFs determine the complementary characteristics of the filter. That is, a lowpass filter can be transformed into a highpass

filter or vice versa, and a bandpass filter can be transformed into a bandstop filter or vice versa; and (ii) For a particular set of phase shifts (ψ_1, ψ_2) of the FOAZPFs, the tuning parameters (i.e., the phase shifts $\varphi_1 = \varphi_2$, ϕ_1 and ϕ_2) of the FOAPPFs determine the bandwidth characteristics of a particular filter type (i.e., lowpass, highpass, bandpass or bandstop).

3.6 Magnitude Responses of Tunable PFs with Variable Bandwidth and Fixed Centre Frequency Characteristics

Figure 6 and *Figure 7* show the squared magnitude responses of the lowpass [*Figure 6*(a)] and highpass [*Figure 6*(b)] and bandpass [*Figure 7*(a)] and bandstop [*Figure 7*(b)] tunable PFs with variable bandwidth and fixed centre frequency (i.e., $\delta_0 = 0$) characteristics. *Figure 6* shows that the bandwidth of each filter type (lowpass or highpass) can be varied from $\omega_c T/\pi = 0.4$ to $\omega_c T/\pi = 0.8$ by varying the phase shifts of the FOAPPFs (i.e., $\varphi_1 = \varphi_2$, ϕ_1 and ϕ_2) and by keeping the phase shifts of the FOAZPFs unchanged (i.e., $\psi_1 = \psi_2 = \pi$ for lowpass and $\psi_1 = \psi_2 = 0$ for highpass), see *Figure 4*. Similarly, *Figure 7* shows that the bandwidth of each filter type (bandpass or bandstop) can be varied from $(\omega_{c2} - \omega_{c1})T/\pi = 0.2$ to $(\omega_{c2} - \omega_{c1})T/\pi = 0.6$ by varying the phase shifts of the FOAPPFs (i.e., $\varphi_1 = \varphi_2$, ϕ_1 and ϕ_2) and by keeping the phase shifts of the FOAZPFs unchanged (i.e., $(\psi_1 = 0, \psi_2 = \pi)$ for bandpass and $(\psi_1 = 3\pi/2, \psi_2 = \pi/2)$ for bandstop), see *Figure 5*. Note that the normalised centre frequencies are designed at $\omega T/\pi = 0$ for the lowpass and highpass filters and at $\omega T/\pi = 0.5$ for the bandpass and bandstop filters.

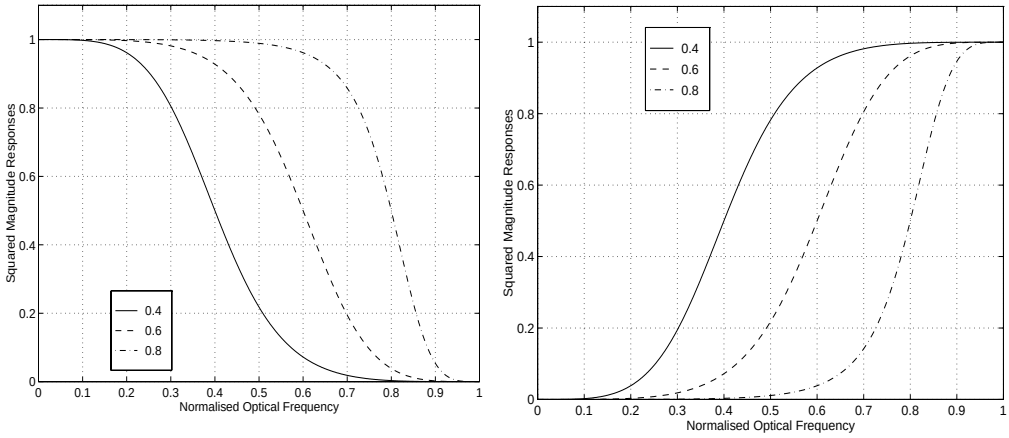

(a) (b)

Figure 6 Squared magnitude responses of the lowpass and highpass tunable PFs with variable bandwidth and fixed centre frequency (i.e., $\delta_0 = 0$) characteristics. (a) Lowpass. (b) Highpass. The numbers inside the legend box represent the normalised 3-dB cutoff frequencies (i.e., $\omega_c T/\pi$), which also correspond to the normalised filter bandwidths. Note that the normalised centre frequency is designed at $\omega T/\pi = 0$.

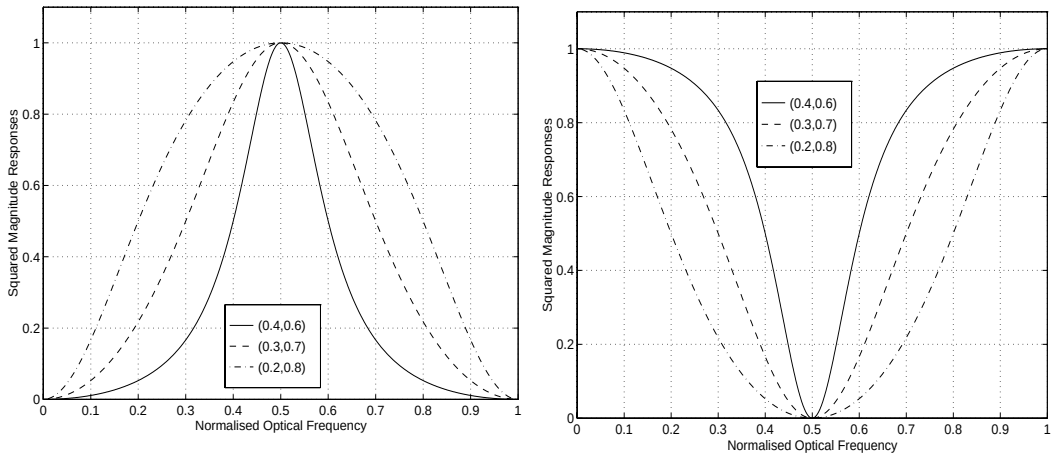

(a) (b)

Figure 7 Squared magnitude responses of the bandpass and bandstop tunable PFs with variable bandwidth and fixed centre frequency (i.e., $\delta_0 = 0$) characteristics. (a) Bandpass. (b) Bandstop. The numbers inside the legend box represent the normalised 3-dB lower and upper corner frequencies $(\omega_{c1}T/\pi, \omega_{c2}T/\pi)$. The normalised filter bandwidth is given by $(\omega_{c2} - \omega_{c1})T/\pi$. Note that the normalised centre frequency is designed at $\omega T/\pi = 0.5$.

3.7 Magnitude Responses of Tunable PFs with Fixed Bandwidth and Variable Centre Frequency Characteristics

Figure 8 and *Figure 9* show the squared magnitude responses of the lowpass [see *Figure 8*(a)] and highpass [see *Figure 8*(b)] and bandpass [see *Figure 9*(a)] and bandstop [see *Figure 9*(b)] tunable PFs with fixed bandwidth and variable centre frequency (i.e., $\delta_0 = 0.1\pi$) characteristics. The design parameters are exactly the same as those in *Table 3* (or *Figure 4*) for the lowpass and highpass filters and in *Table 4* (or *Figure 5*) for the bandpass and bandstop filters, except that an additional phase shift of $\delta_0 = 0.1\pi$ has been added to the phase shifts of the FOAPPFs [i.e., ϕ_1 and ϕ_2, see Eq. (50)] and to the phase shifts of the FOAZPFs [i.e., ψ_1 and ψ_2, see Eq. (51)].

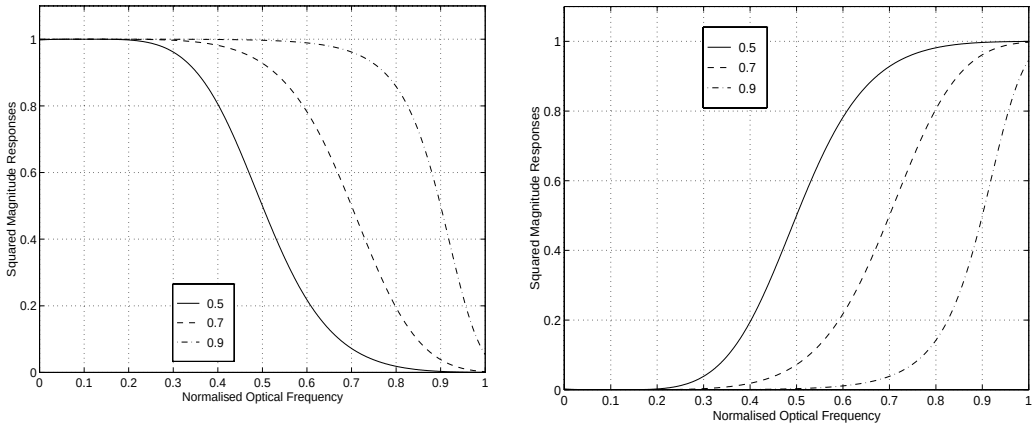

(a) (b)

Figure 8 Squared magnitude responses of the lowpass and highpass tunable PFs with fixed bandwidth and variable centre frequency (i.e., $\delta_0 = 0.1\pi$) characteristics. (a) Lowpass. (b) Highpass. The numbers inside the legend box represent the new normalised 3-dB cutoff frequencies (i.e., $\omega'_c T/\pi = \omega_c T/\pi + \delta_0/\pi$). The normalised filter bandwidths are still the same as those in Figure 6 (i.e., $\omega_c T/\pi = \omega'_c T/\pi - \delta_0/\pi$). Note that the new normalised centre frequency is at $\omega T/\pi = 0.1$.

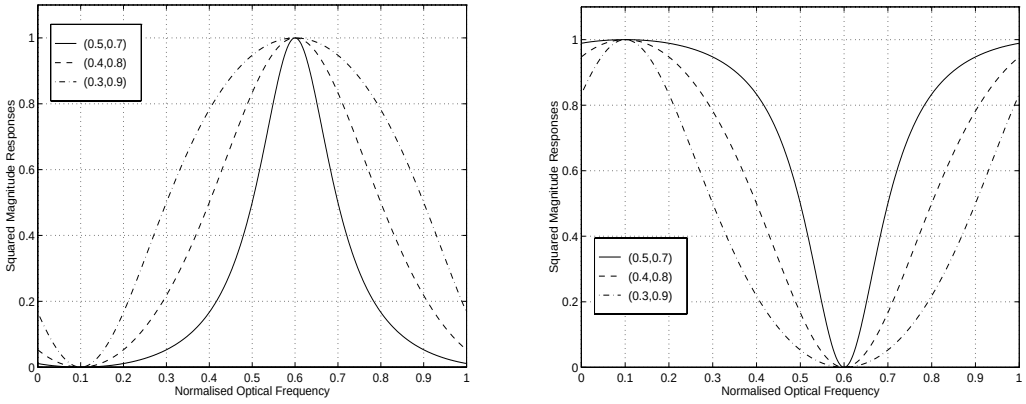

Figure 9 Squared magnitude responses of the bandpass and bandstop tunable PFs with fixed bandwidth and variable centre frequency (i.e., $\delta_0 = 0.1\pi$) characteristics. (a) Bandpass. (b) Bandstop. The numbers inside the legend box represent the new normalised 3-dB lower and upper corner frequencies $(\omega'_{c1}T/\pi, \omega'_{c2}T/\pi)$, where $\omega'_{c1}T/\pi = \omega_{c1}T/\pi + \delta_0/\pi$ and $\omega'_{c2}T/\pi = \omega_{c2}T/\pi + \delta_0/\pi$. The normalised filter bandwidths are still the same as those in Figure 7 (i.e., $(\omega_{c2} - \omega_{c1})T/\pi = (\omega'_{c2} - \omega'_{c1})T/\pi$). Note that the new normalised centre frequency is at $\omega T/\pi = 0.6$.

Figure 8(a) and (b) show that the squared magnitude responses are shifted by $\omega T/\pi = 0.1$ to the right of the frequency axis when compared with the corresponding squared magnitude responses shown in *Figure 6* (a) and (b). The normalised centre frequency has been shifted from $\omega T/\pi = 0$ (*Figure 6*) to $\omega T/\pi = 0.1$ but the corresponding filter bandwidths of *Figure 6* and *Figure 8* remain unchanged. Similarly, *Figure 9*(a) and (b) show that the squared magnitude responses are shifted by $\omega T/\pi = 0.1$ to the right of the frequency axis when compared with the corresponding squared magnitude responses shown in *Figure 7* (a) and (b). The normalised centre frequency has been shifted from $\omega T/\pi = 0.5$ (*Figure 7*) to $\omega T/\pi = 0.6$ (*Figure 9*) but the corresponding filter bandwidths of *Figure 7* and *Figure 9* remain unchanged.

Thus, the centre frequency of a tunable PF can be tuned, without affecting the filter bandwidth, to within one free spectral range by applying an additional phase shift of δ_0 $(0 < \delta_0 < 2\pi)$ to the phase shifters of the FOAPPFs and FOAZPFs. From the point of view of the pole-zero pattern, the effect of δ_0 on the FOAPPFs and FOAZPFs is to rotate the poles and zeros in the angular anticlockwise direction relative to the *z*-plane. As a result, the pole-zero pattern of the resulting tunable PF rotates by some angular movement of δ_0 relative to the *z*-plane, and this has the effect of shifting the filter centre frequency by δ_0 to the right of the frequency axis.

3.8 Summary and comments on Filtering Characteristics of Tunable PFs

As shown in *Figure 4*, the phase shifts of the lowpass (i.e., $\psi_1 = \psi_2 = \pi$) and highpass (i.e., $\psi_1 = \psi_2 = 0$) tunable PFs are out of phase with each other by π. As described in section 3.2, the transfer function $H_{\text{az},k}(z)$ (for the upper output port) and the transfer function $H^*_{\text{az},k}(z)$ (for the lower output port) are out of phase with each other by π. Thus, if the upper output port of the tunable PF has a lowpass magnitude response, then its lower output port has a highpass magnitude response. As a result, the tunable PF can be used as a channel adding/dropping filter which passes certain wavelength channels in one output port, while leaving the other channels undisturbed in the other output port. As shown in *Table 4* and *Figure 5*, the phase shifts ψ_1 and ψ_2 of a particular filter type (bandpass or bandstop[6]) are out of phase with each other by π. As a result, both the output ports of the tunable PF have the same filtering characteristics (bandpass or bandstop). In summary, the filtering characteristics of the tunable PF is shown in *Table 5*.

Output Ports	Filtering Characteristics			
Upper Output Port (Output 1)	Lowpass	Highpass	Bandpass	Bandstop
Lower Output Port (Output 2)	Highpass	Lowpass	Bandpass	Bandstop

Table 5 Filtering characteristics at the output ports of the second-order Butterworth tunable PF.

The largest value of the filter pole, which is limited by the loss of the waveguide loop [see Eq. (48)], is restricted to be $|\hat{p}_k| \le 0.85$ [see Eq. (52)]. As a result, a tunable PF cannot be designed to have a very narrow or broad bandwidth, which requires $|\hat{p}_k| > 0.85$. Thus, the allowable normalised bandwidths of the tunable PF are in the range of $0.1 \le \omega_c T/\pi \le 0.9$ for the lowpass and highpass filters and $0.2 \le (\omega_{c2} - \omega_{c1})T/\pi \le 0.8$ for the bandpass and bandstop filters. These ranges of filter bandwidths are adequate for many filtering applications.

The normalised filter bandwidth can be extended to its full range (i.e., between 0 and 1) by incorporating an erbium-doped waveguide amplifier (EDWA) into the waveguide loop of the FOAPPF to compensate for the loop loss. However, this has the drawback of increasing the cost as well as the complexity of the filter structure, where the latter may degrade the filter performance unless undesirable effects associated with the EDWA are minimised.

Note that the presented design method is applicable to higher-order filters. The roff-off steepness of the magnitude responses of the tunable PF can be increased by increasing the filter order and hence the number of the FOAPPFs and FOAZPFs. However, the lowest filter order should be used to meet a prescribed set of filter specifications to keep the cost and complexity of the filter structure to a minimal.

[6] For the bandstop filter, it has been found from MATLAB that the phase shifts ψ_1 and ψ_2 are only out of phase with each other by π if the normalised centre frequency is at the mid-band frequency (i.e., $\omega T/\pi = 0.5$), which is the case being considered here.

The filter design technique is presented in a general manner and is thus applicable in the design of other types of tunable PFs such as the Chebyshev I and II and elliptic filters, whose properties have been summarised in the Appendix. Obviously, the choice of a particular filter type would depend on specific applications.

4 CONCLUDING REMARKS

• A digital filter design technique has been employed to systematically design tunable PFs with variable bandwidth and centre frequency characteristics as well as lowpass, highpass, bandpass and bandstop characteristics. An *M*th-order tunable PF, which has been designed using integrated-optic structures, consists of a cascade of *M* FOAPPFs with a cascade of *M* FOAZPFs.

• The effectiveness of the PF design method has been demonstrated with the design of the second-order Butterworth lowpass, highpass, bandpass and bandstop tunable PFs with variable bandwidth and centre frequency characteristics. In this design: for a fixed centre frequency, the filter bandwidth can be varied by varying the parameters of the FOAPPFs and by keeping the parameters of the FOAZPFs unchanged, and for a fixed bandwidth, the filter centre frequency can be varied, to within one free spectral range, by adding an additional phase shift to the phase shifters of the FOAPPFs and FOAZPFs.

• As a verification of the technique, an experimental development of the first-order Butterworth lowpass and highpass tunable fibre-optic filters has been carried out. In addition to the Butterworth filters, the proposed filter design technique is applicable to the design of other types of tunable PFs such as the Chebyshev I and II and elliptic filters, depending on the specific application.

ACKNOWEDGEMENT

This work was partially contributed while Dr. Q.N. Ngo was at Monash university. His current address: Photonic Research Centre, School of Electrical and Electronic Engineering, Nanyang Technological University, Singapore.

5 REFERENCES

[1] S. Suzuki, K. Oda, and Y. Hibino, "Integrated-optic double-ring resonators with a wide free spectral range of 100 GHz," *J. Lightwave Technol.,* vol. 13, pp. 1766–1771, 1995.

[2] E. Pawlowski, K. Takiguchi, M. Okuno, K. Sasayama, A. Himeno, K. Okamato, and Y. Ohmori, "Variable bandwidth and tunable centre frequency filter using transversal-form programmable optical filter," *Electron. Lett*., vol. 32, pp. 113–114, 1996.

[3] I. P. Kaminow, P. P. Iannone, J. Stone, and L. W. Stulz, "FDMA-FSK star network with a tunable optical filter demultiplexer," *J. Lightwave Technol*., vol. 6, pp. 1406–1414, 1988.

[4] A. A. M. Saleh and J. Stone, "Two-stage Fabry-Perot filters as demultiplexers in optical FDMA LAN's," *J. Lightwave Technol*., vol. 7, pp. 323–330, 1989.

[5] M. Kuznetsov, "Cascaded coupler Mach-Zehnder channel dropping filters for wavelength-division-multiplexed optical systems," *J. Lightwave Technol*., vol. 12, pp. 226–230, 1994.

[6] N. Q. Ngo and L. N. Binh, "Novel realization of monotonic Butterworth-type lowpass, highpass and bandpass optical filters using phase-modulated fiber-optic interferometers and ring resonators," *J. Lightwave Technol*., vol. 12, pp. 827–841, 1994.

[7] N. Q. Ngo, X. Dai, and L. N. Binh, "Realization of first-order monotonic Butterworth-type lowpass and highpass optical filters: Experimental verification," *Microwave and Opt. Technol. Lett.,* vol. 8, pp. 306–309, 1995.

[8] R. E. Bogner and A. G. Constantinides, *Introduction to Digital Filtering*, London: John Wiley & Sons, 1975.

[9] A. V. Oppenheim and R. W. Schafer, *Discrete-time signal processing*, Englewood Cliffs, NJ: Prentice-Hall, 1989.

[10] T. W. Parks and C. S. Burrus, *Digital Filter Design*, New York: John Wiley & Sons, 1987.

[11] R. E. Bogner and A. G. Constantinides, *Introduction to Digital Filtering*, London: John Wiley & Sons, 1975.

6 APPENDIX : FUNDAMENTAL CHARACTERISTICS OF RECURSIVE DIGITAL FILTERS

It is essential that the fundamental properties of various design techniques and general characteristics of recursive (or IIR) digital filters are summarised for readers who are unfamil;iar with these filters. Further details can be found in references [9], [10], [11]. This basic knowledge is required for the design of tunable PFs as decribed in this report.

6.1 IIR Filter Design Techniques

The common approach to the design of recursive digital filters involves the transformation of a recursive analog[7] (or continuous-time) filter into a recursive digital filter for a given set of prescribed specifications. This is due to the availability of well-developed techniques for analog filters which are often described by simple closed-form design formulas. In such transformations, the essential properties of the frequency response of the analog filter are preserved in the frequency response of the resulting digital filter. The two well-known techniques used for converting Butterworth, Chebyshev I and II, and elliptic analog filters to their corresponding digital filters are the impulse invariance and bilinear transformation methods.

In the impulse invariance method, the impulse response of a digital filter is determined by sampling the impulse response of an analog filter. This technique requires the analog filter to be bandlimited to avoid the aliasing (or interference) effect and thus is only effective for lowpass and bandpass analog filters. If it is to be used for highpass and bandstop analog filters, then additional bandlimiting is required on these filters to avoid severe aliasing distortion.

The bilinear transformation method involves an algebraic transformation between the variables *s* and *z* that maps the entire imaginary axis in the *s*-plane to one revolution of the unit circle in the *z*-plane. Thus, a stable analog filter (with poles in the left half-side of the *s*-plane) can be transformed into a stable digital filter (with poles inside the unit circle in the *z*-plane). As a result, unlike the impulse invariance method, this method does not suffer from the effect of aliasing distortion. However, it suffers from the effect of nonlinear compression of the frequency axis and thus is only useful if this undesirable effect can be tolerated or compensated for.

An alternative approach, which is valid for both the impulse invariance and bilinear transformation methods, is to design a digital prototype lowpass filter and then perform a frequency transformation on it

[7] Analog filters are commonly designed using standard approximation methods, namely, the Taylor series approximations and the Chebyshev approximations in various combinations. Specifically, these approximation methods are used to approximate the desired frequency responses of four different types of analog filters, namely, the Butterworth, Chebyshev I and II, and elliptic filters.

to obtain the desired lowpass, highpass, bandpass and bandstop digital filters. However, the use of the frequency transformation technique in the design of a digital filter is not so straightforward because the analog prototype lowpass filter is generally not known to the designer. Thus, it is necessary to "find" an analog prototype lowpass filter such that, after transformation, the resulting digital filter would meet a given set of specifications. Rapid advances in the field of digital signal processing in recent years led to digital filter design techniques with standard functions in MATLAB[8]. The design of the digital filters and hence tuneable optical filters described in this paper

6.2 Properties of Recursive Digital Filters

The three common types of recursive digital filters are the Butterworth, Chebyshev I and II, and elliptic filters, and their properties are summarised as:

- Butterworth digital filters: They are characterised by a magnitude response that is maximally flat in the passband and monotonic overall. They sacrifice roll-off steepness for monotonicity in the passband and stopband. If the Butterworth filter smoothness is not required, a Chebyshev or an elliptic filter can generally provide steeper roll-off characteristics with a lower filter order.

- Chebyshev I and II digital filters: Chebyshev I filters are equiripple in the passband and monotonic in the stopband, while Chebyshev II filters are monotonic in the passband and equiripple in the stopband. Chebyshev I filters roll off faster than Chebyshev II filters but at the expense of passband ripple. Chebyshev II filters have stopbands which do not approach zero like Chebyshev I filters but are free of passband ripple. Both the Chebyshev I and II filters have the same filter order for a given set of filter specifications.

- Elliptic digital filters: They are equiripple in both passband and stopband. They offer steeper roll-off characteristics than the Butterworth and Chebyshev filters but suffer from passband and stopband ripples. In general, elliptic filters, although the most expensive to compute, will meet a given set of filter specifications with the lowest filter order.

These types of digital filters have zeros located on the unit circle in the z-plane (i.e., $|z| = 1$), which greatly simplify the design of tunable optical filters.

6.3 Transfer Function of Recursive Digital Filters

For analytical clarity, the variables with a cap [e.g., $\hat{H}(z)$] are associated with digital filters while the corresponding variables without a cap [e.g., $H(z)$] are associated with optical filters.

The transfer function of the *M*th-order recursive digital filter can be expressed in a rational form as

[8]MATLAB ™ employs the frequency transformation technique together with the bilinear transformation method with frequency prewarping in the design of the Butterworth, Chebyshev I and II, and elliptic digital filters with lowpass, highpass, bandpass and bandstop characteristics.

$$\hat{H}(z) = \hat{A}\prod_{k=1}^{M}\frac{(z-\hat{z}_k)}{(z-\hat{p}_k)} = \hat{A}\frac{(z-\hat{z}_1)(z-\hat{z}_2)\cdots(z-\hat{z}_M)}{(z-\hat{p}_1)(z-\hat{p}_2)\cdots(z-\hat{p}_M)} \tag{A1}$$

where $\hat{A}$ is a constant and z is the z-transform parameter [25]. Furthermore, $\hat{p}_k$ and $\hat{z}_k$ are the kth pole and zero in the z-plane, which can be expressed in the phasor forms as

$$\hat{p}_k = |\hat{p}_k|\exp(j\arg(\hat{p}_k)) \qquad (0 \le |\hat{p}_k| < 1), \tag{A2}$$

$$\hat{z}_k = |\hat{z}_k|\exp(j\arg(\hat{z}_k)) \qquad |\hat{z}_k| = 1, \tag{A3}$$

where arg denotes the argument. Note that the system stability requires the poles to be located inside the unit circle in the z-plane as described by the condition given in Eq. (2).

Let the transfer function of the kth-stage first-order all-pole digital filter be defined as

$$\hat{H}_{\mathrm{ap},k}(z) = \frac{1}{(z-\hat{p}_k)} \tag{A4}$$

and the transfer function of the kth-stage first-order all-zero digital filter be defined as

$$\hat{H}_{\mathrm{az},k}(z) = (z-\hat{z}_k) \tag{A5}$$

where the subscripts ap and az denote all-pole and all-zero. The transfer function of the Mth-order all-pole digital filter, which is the transfer function of the cascade of M first-order all-pole digital filters, is given by

$$\hat{H}_{\mathrm{ap}}(z) = \prod_{k=1}^{M}\hat{H}_{\mathrm{ap},k}(z). \tag{A6}$$

The transfer function of the Mth-order all-zero digital filter, which is the transfer function of the cascade of M first-order all-zero digital filters, is given by

$$\hat{H}_{\mathrm{az}}(z) = \prod_{k=1}^{M}\hat{H}_{\mathrm{az},k}(z). \tag{A7}$$

The transfer function of the Mth-order recursive digital filter, as given in Eq. (1), can be written alternatively as

$$\hat{H}(z) = \hat{A}\cdot\hat{H}_{\mathrm{ap}}(z)\cdot\hat{H}_{\mathrm{az}}(z). \tag{A8}$$